Repulsive Atomic Gas in a Harmonic Trap on the Border of Itinerant Ferromagnetism

G. J. Conduit* and B. D. Simons

Cavendish Laboratory, 19, J.J. Thomson Avenue, Cambridge, CB3 0HE, United Kingdom

(Received 7 August 2009; revised manuscript received 26 October 2009; published 12 November 2009)

Alongside superfluidity, itinerant (Stoner) ferromagnetism remains one of the most well-characterized phases of correlated Fermi systems. A recent experiment has reported the first evidence for novel phase behavior on the repulsive side of the Feshbach resonance in a two-component ultracold Fermi gas. By adapting recent theoretical studies to the atomic trap geometry, we show that an adiabatic ferromagnetic transition would take place at a weaker interaction strength than is observed in experiment. This discrepancy motivates a simple nonequilibrium theory that takes account of the dynamics of magnetic defects and three-body losses. The formalism developed displays good quantitative agreement with experiment.

DOI: 10.1103/PhysRevLett.103.200403 PACS numbers: 05.30.Fk, 03.75.Ss, 67.85.−d, 71.10.Ca

The transition between ferromagnetism and paramagnetism with increasing temperature is considered to be a canonical example of a continuous phase transition, and the phenomenon has been firmly established in many materials. The ability to tune the critical temperature through varying pressure presents experimentalists with an opportunity to investigate the novel many-body physics predicted to arise in the vicinity of a quantum critical point [1]. However, whether this phase behavior derives from soft magnetic fluctuations, which are believed to drive the Stoner transition first order [2–4], or is a consequence of coupling to auxiliary degrees of freedom such as lattice vibrations remains a subject of considerable interest and debate [5]. The control afforded by Feshbach resonance phenomena in ultracold degenerate Fermi gases presents a controlled platform from which to explore strongly correlated repulsive Fermi systems, including collective effects from nonequilibrium dynamics and spin textures [6,7], and quantum critical phenomena [1].

Although a few early experiments [8,9] conducted on the repulsive side of the resonance hinted at ferromagnetic behavior [3], these investigations were hindered by the challenges posed by the cold atomic gas setup, with the fixed relative populations of particles, trap confinement, atom loss through three-body interactions, and nonequilibrium physics, rendering the conclusive identification of ferromagnetism impossible. However, in a recent study, Jo *et al.* [10] succeeded in observing the first strong evidence for novel phase behavior, consistent with itinerant ferromagnetism in an atomic gas of $\sim 6.5 \times 10^5$ ^{6}Li atoms. To overcome the obstacle of atom loss through three-body interactions the experiment was carried out under nonadiabatic conditions, with the atoms prepared in the disordered nonferromagnetic state and the magnetic field ramped to the repulsive side of the resonance in 4.5 ms and then held fixed for a further 2 ms. To assess the viability of the experimental design, it is crucial to have detailed predictions for the expected phase behavior in the trap geometry. In the following, we will adopt two stands of investigation. First, it is important to understand what we expect to see in an idealized equilibrium trap geometry. This study provides a benchmark both to assess the current experiment and to guide future studies. However, while this analysis achieves a qualitative agreement with experiment, it also exposes important discrepancies highlighting the need to consider nonequilibrium effects. Second, we turn to address nonequilibrium dynamics to critically analyze the experimental observations and establish strong quantitative agreement between theory and experiment.

An atomic gas at equilibrium provides an ideal platform from which to analyze experiment. For a two-component Fermi gas with a local contact interaction and equal masses, the Stoner Hamiltonian is defined by $H = \int d^3x[\sum_\sigma a_\sigma^\dagger(\hat{\mathbf{p}}^2/2m)a_\sigma + g a_\uparrow^\dagger a_\downarrow^\dagger a_\downarrow a_\uparrow]$, where the atoms are distinguished by a pseudospin index $\sigma \in \{\uparrow, \downarrow\}$. Note that the pseudospin nature of the Fermi degrees of freedom implies that the Hamiltonian remains spin rotationally invariant even in the presence of an external magnetic field. Taking into account all contributions to second order in g, the energy density of the Stoner Hamiltonian for a spatially uniform system can be expressed as [2–4],

$$\varepsilon = \frac{1}{V}\sum_{\mathbf{k},\sigma} \epsilon_{\mathbf{k}} n_\sigma^F(\epsilon_{\mathbf{k}}) + \frac{2k_F a}{\pi\nu V^2} N_\uparrow N_\downarrow - \frac{2}{V^3} \times \left(\frac{2k_F a}{\pi\nu}\right)^2 \sum_{\mathbf{k}_{1,2,3,4}} \frac{n_\uparrow^F(\epsilon_{\mathbf{k}_1}) n_\downarrow^F(\epsilon_{\mathbf{k}_2})[n_\uparrow^F(\epsilon_{\mathbf{k}_3}) + n_\downarrow^F(\epsilon_{\mathbf{k}_3})]}{\epsilon_{\mathbf{k}_1} + \epsilon_{\mathbf{k}_2} - \epsilon_{\mathbf{k}_3} - \epsilon_{\mathbf{k}_4}}, \tag{1}$$

where $n_\sigma^F(\epsilon) = 1/[1 + e^{\beta(\epsilon - \mu_\sigma)}]$ denotes the Fermi distribution, with spectrum $\epsilon_{\mathbf{k}}$, chemical potential μ_σ, and reduced temperature β, N_σ is the number of particles, ν is the density of states at the Fermi surface, k_F is the Fermi wave vector of the corresponding noninteracting system, and the scattering length a fully characterizes the strength of the contact interaction close to resonance. We also set $\hbar = m = 1$. Retaining only the leading interaction correction, $\mathcal{O}(k_F a)$, Eq. (1) recovers the conventional mean-field Stoner theory, which predicts that the transition remains second order down to zero temperature. However, the soft

transverse magnetic fluctuations [11] encoded in the second order term [12] have the effect of driving the ferromagnetic transition first order [2–4] at low temperature.

To address the nonuniform atomic trap geometry, we must determine the free energy density, $f = \varepsilon - \mu[n_\uparrow(\mathbf{r}) + n_\downarrow(\mathbf{r})]$. Here the Lagrange multiplier μ enforces the constraint of a fixed total particle number imposed by the trap geometry. It is also convenient to rotate the basis to the axis of net magnetization $s \in \{+, -\}$. To analyze the spatially inhomogeneous atom distribution we invoke a local density approximation which allows the variational minimization $\frac{\delta f}{\delta n_s(\mathbf{r})}$. This leads to two equations for the effective local chemical potentials $\mu_\pm(\mathbf{r})$ of the majority and minority species in the rotated basis that must be solved self-consistently,

$$\mu_\pm(\mathbf{r}) = \mu - V(\mathbf{r}) - \frac{2k_F a}{\pi\nu} n_\mp^F(\mathbf{r}) + 2\left[\frac{2k_F a}{\pi\nu}\right]^2 \sum_{\mathbf{k}_{1,2,3,4}} n_\mp^F(\boldsymbol{\epsilon}_{\mathbf{k}_2}) \frac{n_\pm^F(\boldsymbol{\epsilon}_{\mathbf{k}_1})\delta(\boldsymbol{\epsilon}_{\mathbf{k}_3} - \mu_\pm) + [n_\pm^F(\boldsymbol{\epsilon}_{\mathbf{k}_3}) + n_\mp^F(\boldsymbol{\epsilon}_{\mathbf{k}_4})]\delta(\boldsymbol{\epsilon}_{\mathbf{k}_1} - \mu_\pm)}{\boldsymbol{\epsilon}_{\mathbf{k}_1} + \boldsymbol{\epsilon}_{\mathbf{k}_2} - \boldsymbol{\epsilon}_{\mathbf{k}_3} - \boldsymbol{\epsilon}_{\mathbf{k}_4}}, \quad (2)$$

within the external confining potential $V(\mathbf{r}) = \omega\mathbf{r}^2/2$. To provide a reference with experiment [10], we describe the interactions in terms of a dimensionless interaction strength expressed in terms of the Fermi wave vector $k_F^0 a$ at the center of a trapped noninteracting Fermi gas.

We first address the behavior of the cloud size across the range of interaction strengths. Figure 1(b) confirms that, for weak interactions, the root-mean square (rms) cloud size follows the universal scaling relationship $R_0^{\mathrm{rms}}(1 + \frac{1024}{945\pi^2} k_F^0 a)$ that can be derived from Eq. (2). However, fluctuation corrections soon increase the cloud pressure causing it to inflate rapidly to its fully polarized value $2^{1/6} R_0^{\mathrm{rms}}$. As cloud density is suppressed by pressure, the onset of ferromagnetism at the center of the trap takes place at an enhanced interaction strength compared with the uniform system. Second, in Fig. 1(c) we study the total kinetic energy of the atoms, which is in agreement with the mean-field prediction of LeBlanc *et al.* [7]. With increasing interaction strength the local density falls so that the kinetic energy decreases to $\frac{3}{8} E_F^0 (1 - \frac{2048}{945\pi^2} k_F^0 a)$. The fluctuation corrections increase the cloud pressure and reduce the density so driving the kinetic energy downwards still further. The release energy recorded by experiment extrapolated to zero interaction strength is $\sim 0.45 E_F^0$, which is marginally higher than the analytical prediction of $0.375 E_F^0$. This discrepancy could arise through the recovery of interaction energy upon release from the trap, remnant eddy currents in the coils, or nonequilibrium effects. The final experimental probe that we address here is the atom loss rate due to three-body recombination. Integrating the loss rate $\Gamma = \Gamma_0 (k_F a)^6 \int n_+(\mathbf{r}) n_-(\mathbf{r}) \times [n_+(\mathbf{r}) + n_-(\mathbf{r})] d^3 r$ [13] over the trap yields the variation with interaction strength shown in Fig. 1(d). The mean-field case agrees with the prediction of LeBlanc *et al.* [7]. The initial rapid rise in the loss rate can be attributed to the increase in the $(k_F^0 a)^6$ coefficient, through the universal relation $\Gamma/\Gamma_0 \approx 7(k_F^0 a)^6 \mu^6 / 288\pi^4 \omega^{3/2}$. The later decay in the loss rate is due to the suppression of the product $n_+(\mathbf{r}) n_-(\mathbf{r})$ with the onset of magnetization.

Although there is reasonable qualitative agreement between theory and experiment, a marked divergence arises in the experimental prediction of the interaction strength at the onset of ferromagnetism at $k_F a \approx 2.2$. The theoretical prediction from mean-field theory is $k_F a \approx 1.9$, whereas it is at $k_F a \approx 1.1$ if fluctuation corrections are taken into account. This discrepancy prevents us from drawing a definitive conclusion on whether the transition is first or second order. However, in future experimental studies, it should be possible to gain insight into this question by studying the momentum distribution of the atoms shown in Fig. 2. The latter can be directly measured by studying the spatial distribution following a ballistic expansion [14]. A single noninteracting atomic species has the momentum distribution $n_k \propto k^2 (2\mu - k^2)^{3/2}$. In the partially polarized regime the atomic gas will be ferromagnetic in the high density regions—at the center of the trap. Since the transition from an unpolarized to a fully polarized gas takes place over a small range of interaction strengths, the atomic gas will be partially polarized over a small range of radii. The remainder of the gas is unpolarized. The thin shell of partially polarized gas gives rise to a sharp double peak structure in the momentum distribution in both the mean-field case and also when fluctuation corrections are taken into account. However, the mean-field ferromagnetic transition takes place over a larger range of radii than the fluctuation corrected case, which smears out the double peak feature.

To assess whether the observed experimental phenomenology [10] is consistent with the development of itinerant ferromagnetism, it is important to understand the source of the discrepancy in the predicted interaction strength. In doing so, we will exploit the marginally adiabatic nature of the experiment to explore the quench dynamics of the transition. This necessitates taking into account two contributing factors: how the ferromagnetic state condenses out of the normal phase, and the renormalization of the interaction strength due to three-body losses. The emergence of the ferromagnetic state is nontrivial since the propagation of the condensed spin alignment is bounded by the spin wave velocity. The quench propels the system deep into the ferromagnetic regime, so monopole defects are condensed out from the paramagnetic phase [15,16]. As the defects grow they mutually annihilate, delaying the formation of the ferromagnetic phase, which in turn increases the effective interaction strength required to observe ferromagnetic phenomena. The second component of our dynamical

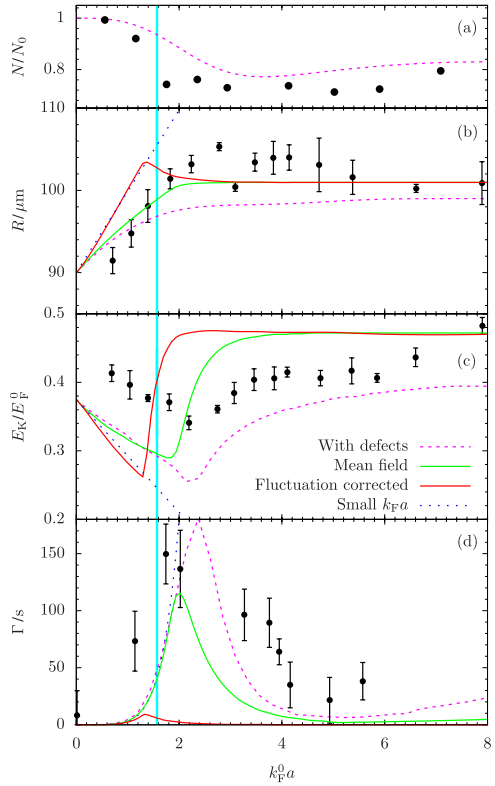

FIG. 1 (color online). (a) Atoms remaining after the hold time, (b) rms cloud size, (c) release energy, and (d) loss rate with the dimensionless interaction parameter $k_F^0 a$ shown on the primary x axis in the mean-field case (green or dark gray), with fluctuation corrections (red or dark gray), and with defects (dashed magenta line). The dotted blue line shows the trend in the small $k_F^0 a$ limit, the vertical cyan line at $k_F^0 a = \pi/2$ is the Stoner criterion, and the experimental points of Ref. [10] are also highlighted.

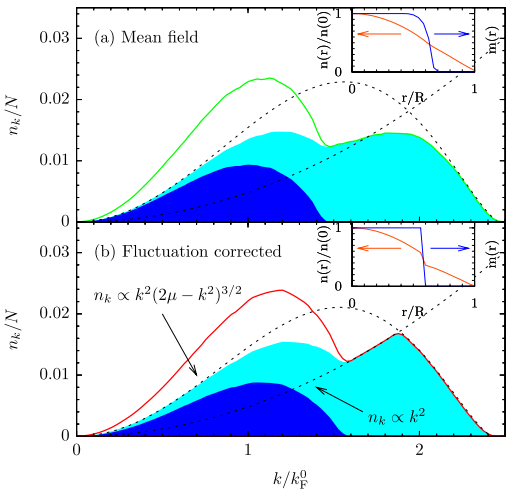

FIG. 2 (color online). The momentum distribution n_k/N of a half net polarized atomic gas in (a) the mean-field case and (b) with fluctuation corrections. The cyan or gray filled curve shows the population of majority spin particles and the blue or dark gray filled curve shows the minority spin particles. The dotted curves show the expected distribution for the majority spin particles in a harmonic trap, $n_k \propto k^2(2\mu - k^2)^{3/2}$, and simply due to the density of states, $n_k \propto k^2$. The inset curves show the radial distribution of atoms (orange or gray, primary y axis) and magnetization (blue or dark gray, secondary y axis).

study is three-body interactions. These reduce the atom density and therefore abate the effective interaction strength $k_F a$, which to compensate must be artificially raised to observe ferromagnetism. The interplay between these two dynamical effects is expected to raise the interaction strength required to observe ferromagnetism to be more in accord with the experimental findings. We now detail how to separately incorporate these effects into a description of the atomic gas, before merging them into a single formalism. Since the characteristic time scale associated with temperature, 0.5 ms, is similar to time scales of the Ketterle experiment [10], we can treat the atomic gas as if it were at zero temperature. Because of the short time scale of the quench, for simplicity we can focus attention on just the mean-field component of the theory [17] and make the approximation that the ferromagnetic transition takes place at the Stoner criterion $k_F a_{\mathrm{CRIT}} = \pi/2$.

The ferromagnetic quench deep beyond the spinodal line leads to the condensation of topological monopole defects [15]. In each defect the spins radiate out from a central core with magnetization $\phi(r > \xi) = \phi_0(1 - \xi^2/r^2)$, where $\xi = 1/k_F\sqrt{k_F a/k_F a_{\mathrm{CRIT}} - 1}$ is the healing length. A uniform atomic gas would be only partially polarized over a range of interaction strengths $\Delta \approx 0.29$, so therefore during the field ramp over time t_{ramp} to a target interaction strength $k_F a_{\mathrm{AIM}}$, the gas will be partially polarized for the time $t_{\mathrm{ramp}}\Delta/k_F a_{\mathrm{AIM}}$. The study of Babadi [17] shows that after this characteristic quench time the defects will adopt an initial size $L_0 = [(\hbar/m k_F^{0\,3/2}/6\pi^2) t_{\mathrm{ramp}}\Delta/k_F a_{\mathrm{AIM}}]^{1/3}$. Subsequently, the defects grow and annihilate as they compete to select the equilibrium spin. This expansion of the defects can be summarized by the growth law of $\sqrt{\hbar t/m}$ [16]. Combined with the initial condensed size of the defects, we therefore model the defect size by $L(t) = \lambda(L_0 + \sqrt{\hbar t/m})$, with λ being an unknown dimensionless constant that we include to account for the system dependent dynamics that go beyond the current analysis.

Having captured defect growth in the model, we now incorporate it into a formalism that also accounts for the atom loss due to three-body interactions. We employ the standard atom loss rate formula [13] to describe three-body recombination $\dot{n} = -111(na^3)^2\bar{\epsilon}n_\uparrow n_\downarrow/\hbar n$, where $\bar{\epsilon} = 4.56\hbar^2 n^{2/3}/m$ is the average kinetic energy. The fall in loss rate due to Pauli blocking is described by a geometric term that can be expressed in terms of the magnetization ϕ through $n_\uparrow n_\downarrow/n^2 = (n^2 - \phi^2)/4n^2$. As the spins within a defect are not parallel, three-body recombination occurs within a defect, which can be expressed through the geometric term as $n_\uparrow n_\downarrow/n^2 = \xi^2/2r^2 + \mathcal{O}(\xi^4)$. Integrating this loss over one defect predicts a net loss rate of

$$\frac{4\pi L^3(t)}{3}\frac{dn}{dt} = -111n(na^3)^2\frac{\bar{\epsilon}}{\hbar}\int_{L(0)}^{L(t)}\frac{\xi^2}{4r^2}4\pi r^2 dr$$
$$\frac{dn}{dt} = -0.144\frac{\hbar}{m}n^{5/3}(k_F a)^6[L(t)-L(0)]\xi^2 L^{-3}(t). \quad (3)$$

Starting in the disordered regime, following the magnetic field ramp we numerically propagate the atom loss forwards in time. If the system breaks into the ferromagnetic regime, $L(t)$ starts to grow as the defects expand and annihilate. Should atom loss cause the system to reenter the normal regime we immediately revert to the $L = 0$ limit. To determine the atomic distribution within the trap we self-consistently evaluate the local effective potential following the method outlined in Eq. (2).

In Fig. 1(a) we first analyze the population of remnant atoms following the field ramp. At weak interaction strengths the number of atoms lost to three-body recombination scales as $\sim(k_F^0 a)^6$. However, the more rapid onset of ferromagnetism and smaller core length conspire to cut losses. Deep within the ferromagnetic regime, around 80% of the atoms remained in the experiment [10], which was used to calibrate the constant $\lambda = 5$. Having determined the dimensionless constant, we now monitor the ramifications of this choice on the growth of the defects. The ratio of the defect size to the core radius, L/ξ, after the hold time, increases with $k_F a$ due to the proliferation of defects commencing earlier and the falling core radius. The rise of L leads to a fall in the number of defects remaining after the field hold to ~ 8. However, no firm evidence has yet been reported for domain formation in experiment.

Now that we have calibrated the theory against the experimental results we can proceed to compare the other physical observables against the experimental data. We first look at the rms cloud size in Fig. 1(b). In the weakly repulsive regime the cloud size increases with interaction strength due to the enhanced pressure between atoms. However, at interaction strengths $1 < k_F^0 a < 2.2$ the increasing atom loss dominates, causing the cloud to shrink. The characteristic minimum formed is in accord with the experimental results, and critically is delayed until the interaction strength $k_F^0 a \approx 2.2$, both because the loss of atoms hinders the onset of ferromagnetism, and since on the border of ferromagnetism the longer core length increases atom loss. Upon ferromagnetic ordering the atom loss falls off causing the cloud to reexpand, which eventually exceeds its original radius. With weak interactions the kinetic energy in Fig. 1(c) falls both as atoms are lost and the cloud dilates. Upon reaching the critical interaction strength of $k_F^0 a \approx 2.2$ ferromagnetic ordering takes place and the kinetic energy rises as the ordered atoms posses a larger Fermi surface. Across the whole range of interaction strengths the theoretical prediction for the kinetic energy falls short of the experimental results, which could be due to the gas being inherently out of equilibrium, recovery of some interaction energy upon release from the trap, or remnant eddy currents in the coils. At high interaction strength the kinetic energy continues to rise as the atom loss decreases, indicative of the upturn seen in the experimental results. Finally, in Fig. 1(d) we address the atom loss rate which climbs strongly as $\sim(k_F^0 a)^6$ before the onset of ferromagnetism. Consistent with the other experimental probes, the peak atom loss is delayed until $k_F^0 a \approx 2.2$. Following the onset of ferromagnetism the atom loss drops away more slowly than without dynamic effects due to the necessity for the defects to grow and the reduced atom loss during the ramp time.

In conclusion, we have performed a detailed critique of the results of the first experimental signs of ferromagnetism in a cold atom gas. First, we demonstrated that the results are not consistent with the formation of an equilibrium ferromagnetic phase. Second, we demonstrated how the experiment indicates that the ferromagnetic phase is formed through the condensation of defect-antidefect pairs that subsequently undergo mutual annihilation, which delays the formation of the ferromagnetic phase to an enhanced interaction strength of $k_F a = 2.2$.

We thank Eugene Demler, Jonathan Edge, Andrew Green, Zoran Hadzibabic, and especially Gyu-Boong Jo and Wolfgang Ketterle for useful discussions.

*gjc29@cam.ac.uk

[1] J. A. Hertz, Phys. Rev. B **14**, 1165 (1976); A. J. Millis, Phys. Rev. B **48**, 7183 (1993).
[2] A. A. Abrikosov and I. M. Khalatnikov, Sov. Phys. JETP **6**, 888 (1958); F. Mohling, Phys. Rev. **122**, 1062 (1961).
[3] R. A. Duine and A. H. MacDonald, Phys. Rev. Lett. **95**, 230403 (2005).
[4] G. J. Conduit and B. D. Simons, Phys. Rev. A **79**, 053606 (2009).
[5] R. B. Laughlin *et al.*, Adv. Phys. **50**, 361 (2001).
[6] I. Berdnikov, P. Coleman, and S. H. Simon, Phys. Rev. B **79**, 224403 (2009).
[7] L. J. LeBlanc *et al.*, Phys. Rev. A **80**, 013607 (2009).
[8] S. Gupta *et al.*, Science **300**, 1723 (2003).
[9] T. Bourdel *et al.*, Phys. Rev. Lett. **91**, 020402 (2003).
[10] G.-B. Jo *et al.*, Science **325**, 1521 (2009).
[11] D. Belitz *et al.*, Phys. Rev. B **58**, 14 155 (1998); M. Shimizu, Proc. Phys. Soc. London **84**, 397 (1964); D. Belitz, T. R. Kirkpatrick, and T. Vojta, Phys. Rev. B **55**, 9452 (1997); J. Betouras, D. Efremov, and A. Chubukov, Phys. Rev. B **72**, 115112 (2005); D. V. Efremov, J. J. Betouras, and A. Chubukov, Phys. Rev. B **77**, 220401(R) (2008).
[12] G. J. Conduit, A. G. Green, and B. D. Simons, Phys. Rev. Lett. **103**, 207201 (2009).
[13] D. S. Petrov, Phys. Rev. A **67**, 010703(R) (2003).
[14] W. Ketterle and M. W. Zwierlein, arXiv:0801.2500.
[15] A. J. Bray, Adv. Phys. **43**, 357 (1994).
[16] J. S. Langer, *Solids Far from Equilibrium*, edited by C. Godrèche (Cambridge University Press, Cambridge, U.K., 1992).
[17] M. Babadi, D. Pekker, R. Sensarma, A. Georges, and E. Demler, arXiv:0908.3483.